CIMAC CONGRESS 25
ZURICH, MAY 19 – 23, 2025

2025 | 068

# Direct comparison of hydrogen-diesel and methanol-diesel dual direct injection engine combustion

Dual Fuel / Gas / Diesel

Shawn Kook, The University of New South Wales

Yifan Zhao, The University of New South Wales
Xinyu Liu, The University of New South Wales
Qing Nian Chan, The University of New South Wales

## ABSTRACT

Hydrogen and methanol are promising renewable fuels investigated extensively in an effort to reduce carbon dioxide (CO2) emissions from diesel engines. This study provides a direct comparison of dual fuel combustion of the two fuels in the same retrofitted 1-litre single-cylinder diesel engine maintaining a high compression ratio of 17.4. The engine was operated at 1,400 rpm with 2,000 J total energy input corresponding to intermediate load conditions, with fixed combustion phasing (CA50) at 10 °CA aTDC achieved by adjusting the diesel direct injection timing. The injection timing of both hydrogen and methanol was varied between 120 and 0 °CA bTDC to control hydrogen-air and methanol-air charge conditions. From the experiments, hydrogen-diesel and methanol-diesel dual direct injection engines were found to share the same combustion characteristics. For both fuels, variations in the injection timing resulted in three distinct combustion modes: premixed burn mode at early injection timings, partially premixed burn mode at intermediate timings, and diffusion burning mode at late timings. Maximum IMEP and thermal efficiency were observed for the partially premixed combustion mode of both fuels. However, the differences in the performance output were obvious. Compared with the diesel baseline, the premixed or partially premixed hydrogen-diesel burn showed consistently higher IMEP/efficiency due to gas compression and higher flame temperature. However, the methanol-diesel combustion showed lower IMEP/efficiency due to lower calorific value and thus lower flame temperature. Regarding engine-out emissions, both hydrogen-diesel and methanol-diesel achieved less CO2 than the diesel baseline; however, its significance was very different in that 50% hydrogen direct injection achieved up to 58% decrease while 50% methanol direct injection showed a limited success of only 7% reduction. The efficiency-NOx trade-off characteristic was evident for the hydrogen-diesel combustion, which required the diffusion burning mode to keep the NOx at the same or lower level compared with the diesel baseline. By contrast, the lower flame temperature of methanol caused a positive result of lower NOx emissions at any selected injection timings. The hydrogen-diesel combustion achieved smoke and uHC/CO emissions below the detection limit of the analysers. The methanol-diesel combustion also achieved more than 50% smoke reduction from the diesel baseline; however, significantly increased HC/CO emissions remained an outstanding issue.

## 1 INTRODUCTION

Compression ignition (CI) engines have historically been the engine of choice in the maritime transport and shipping industries due to their high thermal efficiency, durability and reliability. However, the dependence on traditional fossil fuels in these engines has been a substantial contributor to environmental degradation, primarily through the emission of carbon dioxide ($CO_2$) and other greenhouse gases. Additionally, these engines emit a variety of detrimental pollutants, including oxides of nitrogen ($NO_x$) and particulate matter (PM), which pose considerable environmental threats. In response to these concerns, there is an increasing drive within the industry to transition towards alternative fuels. Among many promising candidates, hydrogen and methanol are widely investigated and tested fuels, offering the potential to reduce the ecological $CO_2$ footprint of maritime operations significantly [1,2].

Hydrogen is a zero-carbon fuel that, unlike conventional fossil fuels, produces no carbon-based emissions such as CO, $CO_2$ and particulates. This makes it an environmentally appealing alternative fuel, with $NO_x$ emissions as the only combustion byproduct contributing to air pollution. Furthermore, hydrogen's high heat of combustion is advantageous as its heating value is approximately three times higher than diesel, allowing for more energy per unit mass. Due to its low boiling point, however, hydrogen is typically stored and supplied in a gaseous phase [3].

For hydrogen production, renewable energy sources such as solar, wind, tidal and even nuclear power provide feasible options to power water electrolysis, thus enabling green hydrogen generation [4]. In addition to its application as a combustible fuel, green hydrogen can serve as a feedstock for green methanol production. Through catalytic reactions with $CO_2$ captured from the environment or combustion processes, hydrogen can be converted into methanol, which offers a carbon-neutral production pathway [5].

Compared to hydrogen, methanol remains liquid at the standard temperature and pressure, making it easier to transport, store and refuel. Although methanol still contains carbon, it does not contain aromatic compounds or carbon-carbon bonds, making it less likely to form soot particles. With its lower flame temperature, the thermal nitrogen monoxide (NO) formation could be reduced. However, the energy content of methanol is only half that of diesel, and carbon-based emissions are still the main emissions during the combustion process [6].

Both hydrogen and methanol are suitable for use in spark ignition (SI) engines given their high octane ratings [7,8]. With the aim to achieve high thermal efficiency and torque output, efforts are also made to utilise these two fuels in CI engines. The auto-ignition of pure hydrogen or methanol in CI engines is challenging. For example, neat hydrogen and methanol require very high compression ratios of 32 and 27, respectively, to cause auto-ignition. Although higher efficiencies could be achieved once auto-ignition has occurred, controlling the combustion remains a significant challenge [9,10].

The recently developed dual-fuel concept employs two separate injectors for the main fuel (*e.g.* hydrogen or methanol [11,12]) and pilot diesel fuel injection. In this configuration, the diesel flames serve as an ignition source, facilitating the ignition of either hydrogen-air or methanol-air mixtures. The implementation of port fuel injection (PFI) for hydrogen and methanol is a straightforward method of achieving dual-fuel operation. However, long mixing duration and increased premixed charge condition lead to excessive pressure rise and knocking, and thus, the main energy contributions of hydrogen and methanol are typically limited to 40% and 70%, respectively [11–13]. In the case of hydrogen, gaseous fuel slip and potential backfire further limit the energy substitution ratio. Furthermore, only the carbon-based emissions such as $CO_2$, uHC and smoke were reduced [16] while the higher premixed combustion caused an increase in $NO_x$ emissions [17]. By contrast, methanol port-injected dual-fuel diesel engines showed reduced $NO_x$ emissions [18] thanks to the lower flame temperature of methanol. However, it resulted in increased levels of CO and uHC emissions [19].

The port injection method has been upgraded to a direct injection (DI) method that uses dual direct injection (DDI) of main and pilot fuel. This approach allows more precise and flexible control of hydrogen or methanol delivery in dual-fuel engines and achieves control of mixture distributions [20,21]. In hydrogen-diesel dual direct injection (H2DDI) combustion, backfire is eliminated by adjusting the hydrogen injection timing after the intake valve closure. Also, the late hydrogen injection executed after pilot diesel injection achieves a reduced peak pressure and heat release rate similar with diffusion flame burning to reduce $NO_x$ emissions. By using the H2DDI method, the hydrogen energy fraction achieved up to 90%, and the $CO_2$ reduction was reduced by 77% compared to the diesel baseline [22].

Such diffusion flame burning could also be achieved with methanol as a main fuel – *i.e.*, the methanol-diesel dual direct injection (MDDI)

combustion with up to 95% energy substitution demonstrated [23]. By advancing the methanol injection timing, the ignition delay was extended and premixed combustion was enhanced; however, $NO_x$ emissions were found to remain below the diesel baseline thanks to lower methanol flame temperature [24]. The drawback was found that CO and uHC emissions were increased, suggesting increased wall-wetting [25].

The existing literature indicates that using hydrogen and methanol as alternative fuels not only assists in reducing the reliance of CI engines on fossil fuels but also holds significant potential for improving engine-out emissions. The concept of dual direct injection has been identified as a promising approach for enabling CI engines to transition into both hydrogen-diesel and methanol-diesel dual-fuel modes. The present study aims to provide valuable insights into the development of heavy-duty engine applications by conducting a direct comparison of hydrogen-diesel and methanol-diesel dual direct injection combustion in the same engine. The experimental investigations were conducted in a modified 1-litre single-cylinder diesel engine by employing dual direct injection with the original diesel injector and additional hydrogen or methanol injector that are interchangeable. The injection timing for hydrogen and methanol ranging from 120 to 0 °CA before the top dead centre (bTDC) was tested to control the mixture distributions and primary combustion mode.

## 2. EXPERIMENTS

### 2.1 Dual Direct Injection Engine Setup

The dual direct injection engine performance and emissions testing were conducted in a single-cylinder engine, modified from a production inline six-cylinder diesel engine, as illustrated in Figure 1. The engine and injection system specifications are summarised in Table 1. The test engine retains the original engine head with only modifications for installing an additional direct injector in the active cylinder. The engine has a bore of 100 mm and a stroke of 125 mm, resulting in a 981.7 $cm^3$ displacement volume. The engine operates under naturally aspirated and unthrottled conditions and has a compression ratio of 17.4. The intake and exhaust pipes are connected to two large surge tanks of 60 $dm^3$ volume to dampen the pressure oscillations associated with single-cylinder operation.

The active cylinder is equipped with the original diesel injector, and an additional direct injector is installed for both H2DDI and MDDI operations, as illustrated in Figure 2. One 8-hole solenoid common-rail diesel injector (Bosch CRIN2-16) with 136 µm diameter measured for each nozzle hole is centrally mounted, and the diesel fuel is pressurised by a high-pressure pump (Bosch CP3). For hydrogen and methanol direct injection, a commercial 6-hole, spray-guided gasoline direct injector (Bosch HDEV6) was mounted, and a nozzle cap was added for 1-mm single-hole injection of hydrogen [26] or 0.2-mm three-hole injection of methanol [24]. The hydrogen or

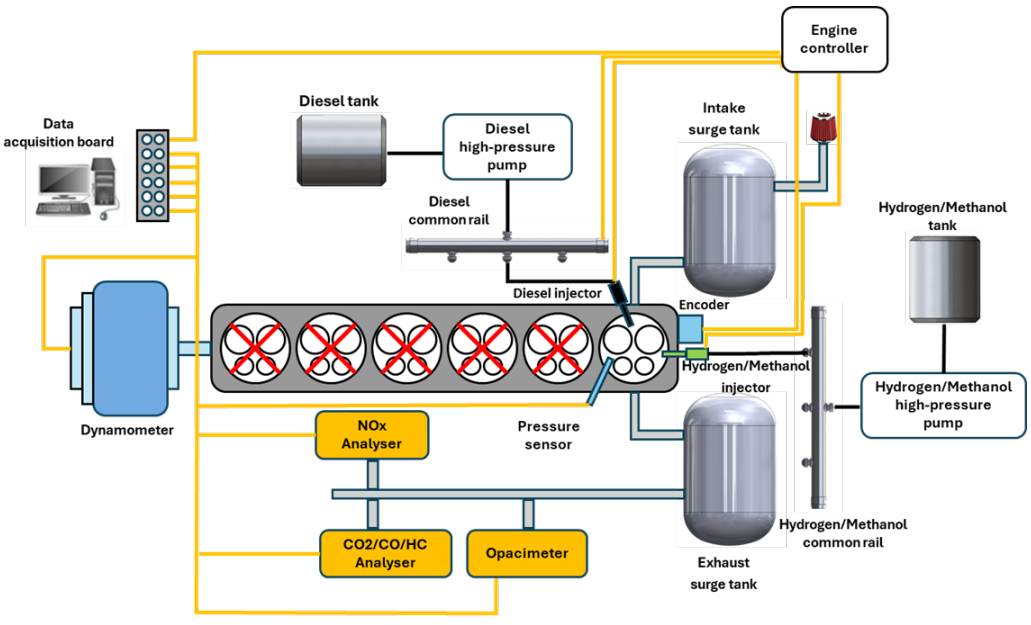


Figure 1. Dual direct injection heavy-duty diesel engine setup

Table 1. Engine specifications

| | | |
|---|---|---|
| Displacement [cm³] | 981.7 | |
| Bore [mm] | 100 | |
| Stroke [mm] | 125 | |
| Compression ratio | 17.4 | |
| Number of valves | 2 intake and 2 exhaust | |
| Injection system | Diesel | Common-rail pump (Bosch CP3.3)<br>Common-rail injector (Bosch CRIN2-16)<br>Number of holes: 8<br>Nominal hole diameter: 136 µm |
| | Hydrogen | Hydrogen Boost Pump (Haskel AG-62)<br>Hydrogen injector: Modified from a conventional GDI injector (Bosch HDEV6)<br>Nozzle: Single hole with 1 mm diameter |
| | Methanol | Pneumatic liquid pump (Maximator M72LVE)<br>Methanol injector modified from the same spray-guided GDI injector<br>Nozzle: Three holes with 200 µm diameter and 60° included angle |

Table 2. Engine operating conditions

| | | |
|---|---|---|
| Engine speed [rpm] | 1400 | |
| Intake air pressure [kPa] | 101.3 (Natural aspiration) | |
| Intake air temperature [K] | 300 | |
| Coolant (water) temperature [K] | 363 | |
| Combustion phasing [CA50, °CA aTDC] | 10 ± 0.5 | |
| Total energy input [J/cycle] | 2000 | |
| Fuel | Hydrogen or Methanol | Diesel |
| Injection pressure [MPa] | 35 | 100 |
| Injection mass [mg] | 8.33 or 50.764 | 22.73 |
| Injection duration [°CA] | 34~40 or 23~25 | 4.28 |
| Injection timing [°CA bTDC] | 0, 10, 20, 40, 60, 120 | 1 - 7 |
| Energy fraction [%] | 50 | 50 |

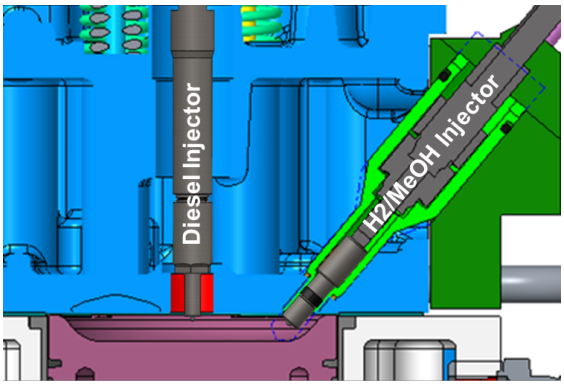


Figure 2. Patented dual direct injector method illustration [24,26]

methanol injector mounted on the cylinder head was 48° tilted to the engine head bottom plane. The maximum injection pressure for both gases hydrogen and liquid methanol injectors was 35 MPa. The hydrogen injection pressure was controlled using a boost pump system (Zenobalti ZB-1301) based on a single-stage, single-acting pneumatic hydrogen pump (Haskel AG-62-86979), and the methanol injection pressure was achieved using a single-stage, single-acting pneumatic liquid pump (Maximator M72LVE).

### 2.2 Engine Instrumentation

The test engine was equipped with a piezoelectric pressure transducer (Kistler 6056A with amplifier 5015A) mounted on the cylinder head to monitor the real-time in-cylinder pressure. A rotary encoder was used (Autonics E40S8, 1800 pulses per revolution) to detect the crankshaft position, and the engine speed was regulated by an eddy current dynamometer (FroudeHoffmann, AG-30HS). A universal engine controller (Zenobalti, ZB-9013P) was used to control the injection timing and adjust it according to the detected crankshaft position; the same system was used for injection duration control and diesel common-rail pressure control. For replicating a warmed-up engine operation, the coolant temperature was maintained constant at 363 K by using a water heater/circulator (Thermalcare, Aquatherm RQE0920). The engine-out emissions were also measured. $NO_x$ levels were gauged with a chemiluminescent analyser (Ecotech 9841AS, 1% error range). For $CO_2$, CO and uHC, a nondispersive infrared analyser (Horiba MEXA-584L, 1.7% error range) was used. The exhaust opacity was also measured using an opacimeter (Horiba MEXA-600S, 0.15 $m^{-1}$ accuracy of light absorption).

### 2.3 Engine Operation Strategy

The in-cylinder pressure data were recorded for 100 continuous firing cycles for ensemble averaging and statistical analysis. The measured pressure profiles were also used to calculate the apparent heat release rate (aHRR), net indicated mean effective pressure (IMEP), and coefficient of variation (CoV) of IMEP. The combustion phasing parameters of CA10, CA50 and CA90 corresponding to the crank angle position of 10%, 50%, and 90% heat release were also evaluated with which burn duration parameters were derived.

Table 2 summarises the selected engine operating conditions. The engine was run at a constant speed of 1400 revolutions per minute (rpm), at which point the base engine produced the maximum torque. Due to the additional degrees of freedom associated with the two fuel injectors, a fuel-substitution strategy was implemented for this investigation. The total energy injected per cycle was fixed at 2000 J, corresponding to intermediate engine loads. For both hydrogen and methanol, the energy fraction was set at 50%, meaning 50% of the total input energy was provided by hydrogen or methanol for H2DDI or MDDI operation. Further increase of energy substitution was possible – for example, up to 90% in H2DDI [22] and up to 70% in MDDI [24]. However, the achievable maximum load and power output differ depending on the fuel type, which made a direct comparison of H2DDI and MDDI not feasible. For the sake of direct comparison, an identical 50% energy substitution ratio was found to be the most useful. Follow-up studies performed in the same engine will report the results of higher energy substitution ratios of H2DDI and MDDI separately. The measured injection mass of hydrogen and methanol were 8.33 mg and 50.764 mg, respectively. For hydrogen, it was required to inject for 34~40 °CA depending on the injection timing as the back pressure changed. Similarly, methanol injection duration was adjusted between 23 and 25 °CA. To the other half of the energy, diesel was injected at 100 MPa with 22.73 mg of injection mass for the duration of 4.28 °CA. In the case of the diesel baseline, the single injection mass was 45.5 mg for 8.15 °CA injection duration. The hydrogen and methanol injection timings were varied between 120 °CA bTDC and TDC, and the diesel injection timing was adjusted to ensure that the mid-point combustion phasing was kept constant at 10 ± 0.5 °CA after the top dead centre (aTDC).

# 3 RESULTS AND DISCUSSION

## 3.1 In-cylinder Pressure and Apparent Heat Release Rate

Figure 3 shows the ensemble-averaged in-cylinder pressure and apparent heat release rate (aHRR) profiles for the injection timing ranging from 120 to 0 °CA bTDC. The results are shown for both H2DDI (left) and MDDI combustion (right). In each plot, the diesel baseline is shown with a black line, while the hydrogen and methanol injection timing ($H_2$SOI/MSOI) variations are marked using different colours. Specifically, the most advanced injection timing of 120 °CA bTDC is shown in cyan and later injection timings of 60 °CA bTDC in green, 40 °CA bTDC in purple and 20 °CA bTDC in yellow. The most retarded injection timings of 10 °CA bTDC and TDC are plotted with orange and blue coloured lines. To control the midpoint combustion phasing (CA50) at 10 °CA aTDC, adjustments were made to the diesel injection timing (DSOI) noted in the legend box. Only the very late TDC injection case in H2DDI and MDDI combustion failed to achieve this CA50.

The first noticeable difference between H2DDI and MDDI is observed from the TDC pressure. H2DDI shows higher TDC pressure than the diesel baseline with an increasing gap for more advanced

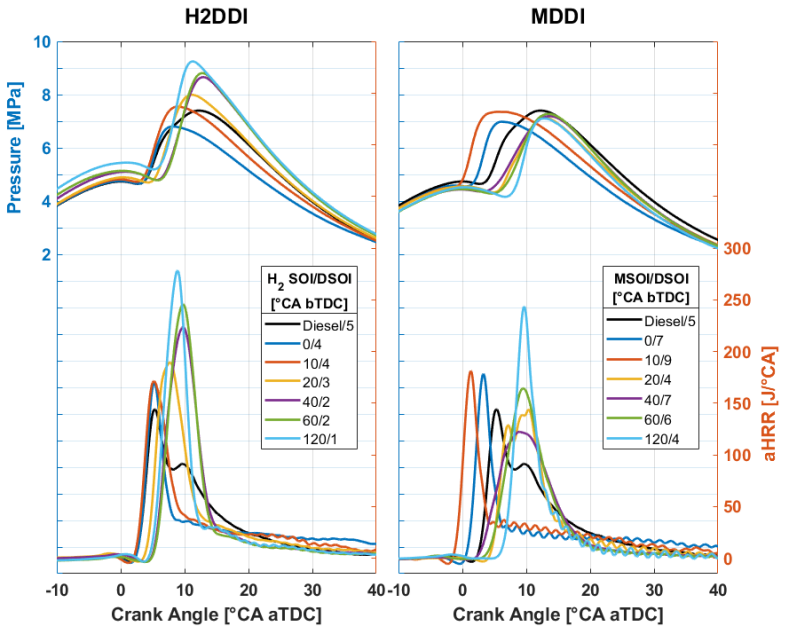


Figure 3. Effect of hydrogen and methanol ($H_2$ and MeOH) injection timing ($H_2$SOI/MSOI) on cylinder pressure and apparent heat release rate (aHRR) at 50% energy fraction in H2DDI (left) and MDDI (right) operation.

hydrogen injection timings. This is expected as the high-pressure gas injection and following compression lead to increased pressure [27]. By contrast, MDDI consistently shows lower TDC pressure than the diesel baseline, which decreases for more advanced methanol injection timing. This direct opposite trend was due to evaporative cooling in that the endothermal phase change of liquid methanol reduced the in-cylinder pressure. For both H2DDI and MDDI, late injection timing caused the TDC pressure to be very similar with the diesel baseline, as the gas compression and evaporative cooling were lacking prior to TDC.

For 120 °CA bTDC injection (cyan line), the increased hydrogen compression led to a significant increase in the peak combustion pressure for H2DDI compared to the diesel baseline. However, MDDI of the same injection timing shows lower peak combustion pressure as the start of combustion was delayed due to the evaporative cooling, and thus, it occurred later in the expansion stroke. The same trend is observed for later 60 and 40 °CA bTDC when H2DDI and MDDI are compared. For both H2DDI and MDDI, the magnitude of peak aHRR decreases with more retarded injection timings up to 40 °CA bTDC. However, both the peak pressure and aHRR are still higher for H2DDI than the diesel baseline. By contrast, the peak pressure is lower for MDDI, and even the peak aHRR becomes lower than the diesel baseline. From the observed trends, it is plausible to explain the mode of combustion of hydrogen and methanol at this early injection timing range was primarily premixed burn in that the increased charge premixing at earlier injection timing led to higher peak pressure and the profile of aHRR being a single premixed burn peak and little mixing-controlled combustion phase. Due to hydrogen gas compression and methanol evaporative cooling, however, their peak magnitude relative to the diesel baseline was always higher for H2DDI and became lower for MDDI.

As the injection timing of H2DDI was further retarded to 20 and 10 °CA bTDC, the peak pressure continued to decrease, becoming similar with the diesel baseline. The peak aHRR is still higher than the diesel baseline. From this observed trend and the shape of the aHRR profile being a lower peak and higher late-cycle magnitude, a change of the combustion mode was suggested. The hydrogen mixing-controlled combustion phase is dominant with these late injection timings, meaning the primary mode of combustion was a diffusion burning mode. In comparison, MDDI underwent a different trend in the peak pressure and aHRR. They increase as the methanol injection timing is further retarded to 10 °CA bTDC, which was a result of more advanced diesel injection timing required to maintain CA50. The combustion started earlier in the expansion stroke, which caused the higher peak magnitude of pressure and aHRR. However, a mixing-controlled combustion with a lower rate of heat release that lasted longer followed. For 0 °CA bTDC (TDC), it was not possible to fix CA50 at 10 °CA aTDC for both H2DDI and MDDI. This was due to a very low rate of heat release associated with the diffusion

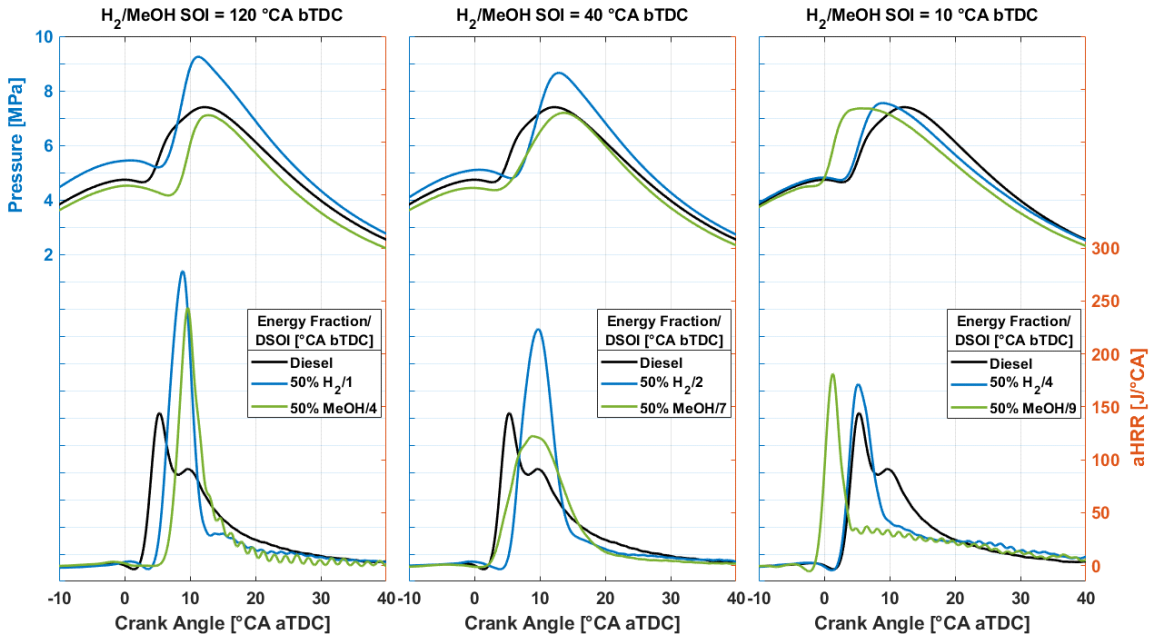


Figure 4. Effect of the hydrogen and methanol fuel type on in-cylinder pressure and apparent heat release rate (aHRR) across three identified typical combustion modes at 50% energy fraction.

burning. As a result, the peak pressure was lower than the diesel baseline for both H2DDI and MDDI. The peak aHRR is observed higher as some premixed portion of hydrogen and methanol burnt, but the following aHRR during the mixing-controlled phase of the combustion is lower than the diesel baseline, which once again indicates diffusion burning of hydrogen and methanol.

One can expect an effective use of the premixed burn mode achieved with early hydrogen and methanol injection timings towards increased efficiency. It is also expected that the diffusion burning mode is utilised to suppress thermal NO formation thanks to the decreased rate of heat release. To further investigate the combustion mode change occurring due to the injection timing, Figure 3 was replotted for each of the three injection timings representative of premixed, partially premixed and diffusion burning modes. Three lines in this figure correspond to H2DDI (blue) and MDDI (green) as well as diesel baseline (black). Figure 4 shows the results. For 120 °CA bTDC injection (left), both H2DDI and MDDI show aHRR profile shapes of the premixed burn. Compared to the diesel baseline displaying a double peak in aHRR – *i.e.* the first peak due to premixed burn and the second peak with a lower magnitude due to the mixing-controlled burn, both H2DDI and MDDI show a single peak aHRR profile associated with the combustion of hydrogen-air or methanol-air change that was mixed prior to the start of combustion and initiated by the diesel flames. Between H2DDI and MDDI, H2DDI shows a higher peak aHRR. The most significant difference is seen in the pressure. The peak pressure of H2DDI is much higher than that of the diesel baseline, whereas the premixed methanol combustion in MDDI shows a lower peak pressure. The increased TDC pressure of H2DDI due to hydrogen compression and decreased TDC pressure associated with evaporative cooling of methanol was thought to be the primary cause.

A very different trend is observed for 10 °CA bTDC injection (right). The pressure before the timing of methanol direct injection is identical for all three cases, and the peak pressure is also measured at about the same level for all three cases. The peak aHRR is still higher for H2DDI and MDDI than that of the diesel baseline. It is, however, noticeable that the difference in peak aHRR becomes much smaller in this diffusion-burning mode. The magnitude of aHRR following the first peak increases for H2DDI and MDDI compared to that of the premixed burn mode (120 °CA bTDC injection), which eventually exceeds the magnitude of diesel baseline at about 20 °CA aTDC. This clearly demonstrates the diffusion burning mode of hydrogen or methanol. Between H2DDI and MDDI diffusion burning, both pressure and aHRR are observed to be similar except that the earlier phasing of MDDI is the only significant difference. This was due to the earlier diesel injection timing required to maintain CA50.

Between the premixed burn-dominant mode achieved with 120 °CA bTDC injection and the diffusion burning-dominant mode of 10 °CA bTDC injection, the intermediate timing of 40 °CA bTDC indicates partially premixed burn as a new mode of combustion. Due to the hydrogen gas compression, the TDC pressure is still higher for H2DDI, and thus, the peak pressure is measured the highest, similar with the premixed burn mode results. However, the difference was reduced significantly. The aHRR profiles still maintain the shape of the premixed burn, but its peak magnitude is significantly reduced and the width is extended. This intermediate behaviour indicates the hydrogen-air and methanol-air charge was partially premixed with an increased portion of the charge burnt through the mixing-controlled combustion, which however, was not dominant as in the later 10 °CA bTDC injection case. Figure 4 confirms that the modulation of the burn mode is possible with dual direct injection technology employing two separate injectors thanks to a full degree of freedom of injection timing control. Between H2DDI and MDDI, the former shows much higher sensitivity to the injection timing changes due primarily to the hydrogen gas compression.

### 3.2 Combustion Phasing and Burn Duration

The aHRR data in Figures 3 and 4 were further processed to show combustion phasing and burn duration parameters, as shown in Figure 5. As mentioned previously (Table 2), CA50 was kept constant at 10 ± 0.5 °CA aTDC by adjusting the diesel injection timing. The exception was found with TDC injection timing for H2DDI and MDDI combustion, at which most hydrogen and methanol injection occurred after 10 °CA aTDC. Therefore, it was not possible to maintain the CA50 regardless of diesel injection timing.

Figure 5 (top-left and top-right) displays the calculated CA10 and CA90, respectively. CA10, marking the start of combustion, is directly influenced by diesel injection timing as an ignition source, showing no distinct trend related to the burn mode or H2DDI / MDDI. Conversely, CA90 exhibits a noticeable trend where early injection results in a lower CA90 due to increased premixed combustion, while very late injection timing led to higher CA90 as the mixing-controlled combustion extended the lower level aHRR throughout the late combustion cycle and prolonged as the fuel injection continued.

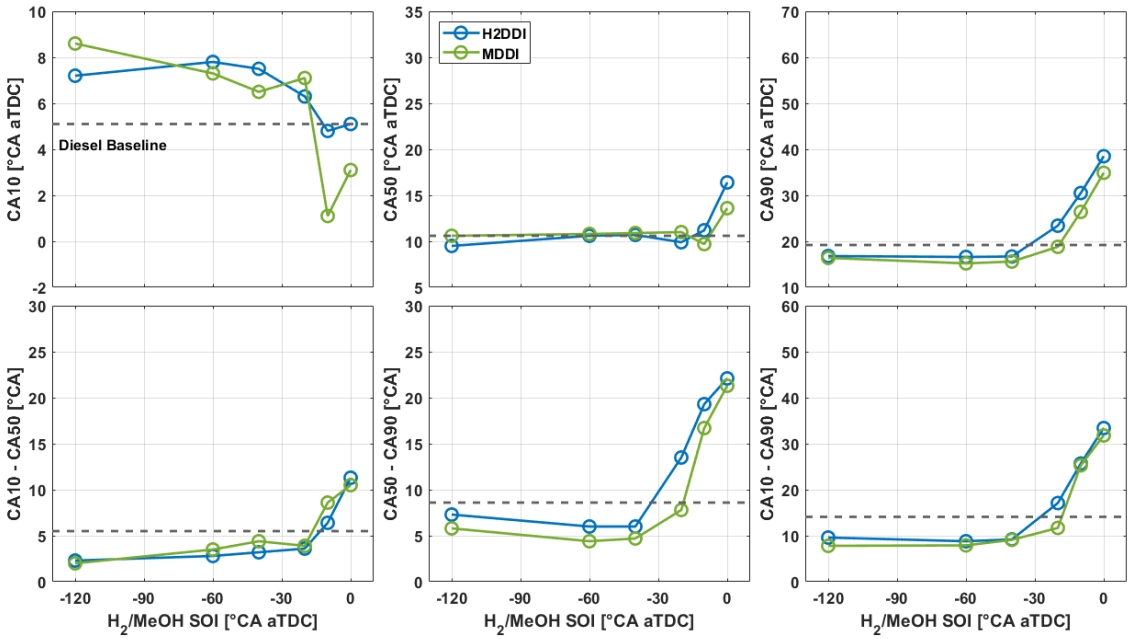


Figure 5. Effect of hydrogen and methanol ($H_2$ and MeOH) injection timing ($H_2$SOI/MSOI) on combustion phasing and burn duration parameters at 50% energy fraction in H2DDI and MDDI operation. The diesel baseline data are denoted in each plot with the grey dashed line.

The burn duration shown in Figure 5 (bottom) reaffirms that both CA50-CA90 and CA10-CA90 are predominantly determined by CA90, reflecting the influence of increased mixing-controlled combustion, which results in longer burn durations. Despite the clarity in burn duration analysis indicating the diffusion burning mode, there is no distinct difference between injection timings associated with the premixed burn (120–60 °CA bTDC injection) and the partially premixed burn (40–20 °CA bTDC injection).

### 3.3 Engine Performance and Stability

In addition to the aHRR parameters derived from the data of Figures 3 and 4, in-cylinder pressure parameters were obtained. Figure 6 shows the results for five different parameters, including the peak pressure, net indicated mean effective pressure (IMEP), net indicated efficiency, ignition delay and coefficient of variation (CoV) of IMEP. From the peak pressure plot, higher peak pressures are observed for H2DDI, which decrease with retarded hydrogen injection timing. By contrast, the peak pressure of MDDI appears insensitive to the methanol injection timing but stays slightly below the level of the diesel baseline. The maximum difference between H2DDI and MDDI is observed at the earliest injection timing of 120 °CA bTDC, at which point the peak pressure of H2DDI is 2.2 MPa higher (an increase of 30%). However, the peak pressure of both H2DDI and MDDI combustion is almost identical in the diffusion burning mode – *i.e.* 10 and 0 °CA bTDC injection. This was expected as the lower rate of heat release occurring from the diffusion flames.

The higher peak pressure does not translate directly to higher power output. The IMEP plot shows the maximum net IMEP is measured at 40 °CA bTDC or roughly in the partially premixed burn mode for both H2DDI and MDDI. It was an optimised condition for sufficiently high pressure to produce high work and prolonged burn duration to maintain the duration of work produced, particularly in the late cycle. Good correspondence to this was previously found from the late-cycle burn duration of CA50-CA90 from Figure 5. Between H2DDI and MDDI, the net IMEP was measured higher for H2DDI at any fixed injection timing. In fact, MDDI exhibits lower net IMEP than the diesel baseline for all injection timings, whereas H2DDI produces higher net IMEP except very late timings of 10 and 0 °CA bTDC (*i.e.* diffusion burning mode). One plausible cause is higher flame temperature of hydrogen than methanol. The trends of the indicated efficiency follow the net IMEP trends simply due to the fixed total energy applied in this study. The diesel baseline measured 38% net indicated efficiency, which could be increased up to 44% with the implementation of H2DDI at 40 °CA bTDC (*i.e.* partially premixed burn). The low efficiency of MDDI due to lower methanol flame temperature is obvious from the plot.

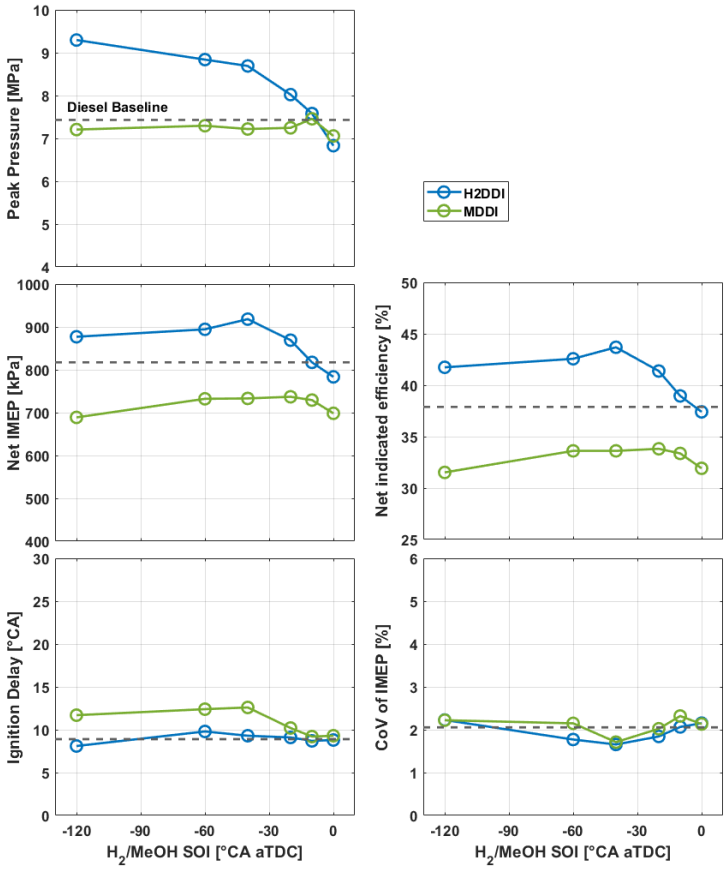


Figure 6. Effect of hydrogen and methanol ($H_2$ and MeOH) injection timing ($H_2$SOI/MSOI) on peak pressure, net indicated mean effective pressure (IMEP), ignition delay, net indicated efficiency, and coefficient of variation of IMEP at the 50% energy fraction in H2DDI and MDDI operation.

One noticeable trend seen in Figure 6 is the longer ignition delay measured for MDDI combustion. As mentioned previously, evaporative cooling of methanol caused increased ignition delay time. By contrast, H2DDI combustion had a shorter ignition delay as the hydrogen gas compression caused increased TDC pressure. Interestingly, the evaporative cooling appears to be affected by the methanol injection timing with earlier injection timing causing extended ignition delay. Hydrogen gas compression has a minimal impact on ignition delay, which was primarily due to diesel injection timing control. That is, the diesel was injected later for more advanced hydrogen injection timing, which balanced off the increased gas compression.

For all the tested conditions, the CoV of IMEP plot delivers a very positive message that the cyclic variance is as of the diesel baseline or lower. The high combustion stability achieved from both H2DDI and MDDI indicates that the combustion control via the diesel injection was effective. It also confirms that both hydrogen and methanol direct injections are not prone to misfiring, even if the diffusion burning mode was dominant with the late injection timings.

### 3.4 Engine-Out Emissions

For hydrogen engines, the engine-out emissions of $NO_x$ are a known major concern. For methanol engines, increased CO and uHC emissions are known issues. Figure 7 shows the engine-out emissions of $NO_x$, CO and uHC, as well as smoke and $CO_2$, for all the tested conditions of the present study. The data was normalised with net IMEP.

The first noticeable trend from Figure 7 is a significant $CO_2$ reduction achieved for H2DDI. From 50% $H_2$ energy combustion – *i.e.* 50% removal of carbon-based fuel, the maximum reduction was measured at 40 °CA bTDC hydrogen injection, realising the partially premixed burn mode. This was primarily due to the increased power output. The $CO_2$ emission is measured at 310.6 g/kWh, a 58% reduction from the diesel baseline (743 g/kWh). However, MDDI shows a much less significant reduction of $CO_2$ emission measured at about a 7% decrease due to its nature of hydrocarbon fuel and lower power output. It is suggested that for the maximum $CO_2$ reduction benefit, methanol should be produced from renewable sources so that the life-cycle $CO_2$

emission could be lowered. One important trend observed for both H2DDI and MDDI is that the $CO_2$ emission does not show high sensitivity to the injection timing variation. This suggests the $CO_2$ reduction was due primarily to the decreased total carbon content in the fuel.

Regarding other air-polluting emissions, the smoke opacity shows zero for H2DDI while a significant reduction was also achieved for MDDI. No smoke from hydrogen combustion was well expected, and the reduced carbon to hydrogen ratio and oxygenated molecular structure in methanol were also found to help reduce the smoke emissions by up to 65% at 40 °CA bTDC (*i.e.* partially premixed burn).

The same benefit of 50% carbon-free fuel use in H2DDI combustion was observed from CO and HC emissions. Simply, the emissions went below the detection limit of the gas analysers and thus no CO and uHC results are plotted. For MDDI operation, however, increased CO and uHC emissions are obvious. This is primarily caused by incomplete combustion due to low flame temperature of methanol, direct injection leading to unburnt fuel in crevice volumes and wall wetting [24,25]. For CO emission, it shows a monotonous decrease with the delayed methanol injection, indicating that diffusion flames were more effective in burning out the remaining mixtures. The uHC emissions also show a decreasing trend with diffusion burning, which is realised with the late injection timing. However, the CO and uHC emissions remain at a higher level, suggesting a clear need for further developments. The extent of unburnt HC and CO emissions in exhaust gases indicates the combustion efficiency, and it measures the incompleteness of the combustion reactions. With the measured CO and HC emissions, the combustion efficiency was estimated as shown in Figure 7(top-right). It was noted the nature of this estimation means the combustion efficiency of H2DDI is 100% as there was no measured CO and uHC emissions. [28,29] The diesel baseline also estimated 99% combustion efficiency due to very low uHC and CO emissions. By contrast, the combustion efficiency for MDDI operation displays a reversed trend of the unburnt HC with a drastic increase of CO emissions at early injection timings attributing to a marked lower combustion efficiency. The trend shown in the estimated combustion efficiency once again suggests the positive effect of diffusion burning in burning out the remaining mixtures.

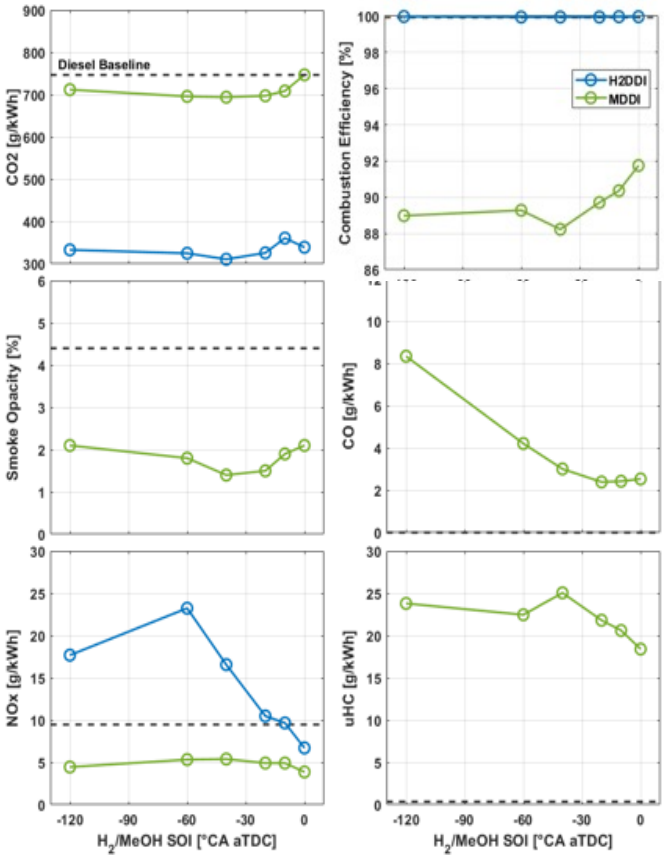


Figure 7. Effect of hydrogen and methanol ($H_2$ and MeOH) injection timing ($H_2$SOI/MSOI) on engine-out emissions of $CO_2$, smoke, $NO_x$, CO, and uHC at 50% energy fraction in H2DDI and MDDI operation. Shown at the top-right is estimated combustion efficiency based on the combustion incompleteness caused by CO and uHC emissions.

A main advantage of MDDI operation is found with $NO_x$ reduction. Figure 7 shows that $NO_x$ emissions of MDDI are half of the diesel baseline. This was a result of the lower flame temperature of the methanol resulting in reduced thermal NO formation. By contrast, H2DDI struggles with increased $NO_x$ emissions, particularly at premixed burn mode realised with early injection timings. The retarded injection timing and partially premixed burn mode could reduce the $NO_x$; however, it is only the late injection timings of 10 and 0 °CA bTDC to achieve the diffusion burning mode for $NO_x$ emissions on par with the diesel baseline or lower. It was noted that 10 °CA bTDC injection of the H2DDI combustion showed the same power output and efficiency (see Figure 6), meaning the same power and $NO_x$ engine operation is possible with H2DDI. In other words, this injection timing is a sweet spot of H2DDI, achieving 50% $CO_2$ reduction while keeping the power output and $NO_x$ at the same level as diesel.

## 4 CONCLUSIONS

The present study was conducted to provide a comparative analysis of the hydrogen-diesel and methanol-diesel combustion in the same dual direct injection engine, termed as H2DDI and MDDI. While varying the injection timing of hydrogen or methanol supplying 50% of total energy input, the in-cylinder pressure, heat release rate and engine-out emissions were directly compared. The main findings of this experimental study are summarised as follows:

- The H2DDI and MDDI combustion were found to exhibit similar shifts in combustion mode with the injection timing altered such that the early injection timing of 120 to 60 °CA bTDC indicated a premixed burn mode characterised by a high-magnitude single peak aHRR profile, and the late injection timings of 10 to 0 °CA bTDC led to a diffusion burning mode with a small peak and longer-lasting low-magnitude aHRR in the late cycle. In between these, 60 to 40 °CA bTDC injection caused a distinct partially premixed burn mode.

- The TDC pressure shows an opposite trend in H2DDI and MDDI combustion. The added hydrogen leads to increased end-of-compression pressure higher than the diesel baseline, whereas the evaporative cooling effect of methanol results in reduced compression pressure. Both effects become minimal at later injection timing. The peak pressure in H2DDI operation is higher and decreases to the level of the diesel baseline with more retarded injection timings, whereas MDDI exhibits less sensitivity to the change in injection timing and always displays peak pressure below the diesel baseline.

- The highest IMEP and efficiency were measured for H2DDI and MDDI combustion under the partially premixed burn mode. The H2DDI combustion shows higher IMEP and efficiency than MDDI while MDDI exhibits lower IMEP than the diesel baseline. This was related to higher flame temperature of hydrogen and gas compression as well as lower flame temperature of methanol as one plausible cause. Regardless of H2DDI or MDDI, the CoV of IMEP was maintained low at 2.5% and below, indicating stable engine operations.

- Both H2DDI and MDDI combustion result in lower $CO_2$ and smoke emissions compared to the diesel baseline; however, the difference between H2DDI and MDDI is significant. Hydrogen's zero-carbon content achieves up to a 58% reduction in $CO_2$ emissions and eliminating smoke completely. Although $NO_x$ emissions present a significant concern, they remain at or below the diesel baseline for late injection timings of 10 to 0 °CA bTDC when the diffusion burning mode was utilised in H2DDI combustion. Conversely, the MDDI combustion produces only about half the $NO_x$ compared to the diesel baseline thanks to the low methanol flame temperature. However, MDDI combustion struggles with higher levels of CO and uHC due to incomplete combustion and potential wall-wetting, issues that are not present in H2DDI combustion.

## ABBREVIATIONS

**aHRR:** Apparent heat release rate

**aTDC**: After the top dead centre

**bTDC**: Before the top dead centre

**°CA**: Crank angle position

**CA10**: Crank angle position of 10% heat release

**CA50:** Crank angle position of 50% heat release

**CA90**: Crank angle position of 90% heat release

**CI**: Compression ignition

**CO**: Carbon monoxide

**CoV**: Coefficient of variation

**$CO_2$**: Carbon dioxide

**DI**: Direct injection

**DDI**: Dual direct injection

**DSOI:** Diesel start of injection timing

**GHGs**: Greenhouse gases

**H2DDI**: Hydrogen-diesel dual direct injection

**$H_2$SOI**: Hydrogen start of injection timing

**IMEP**: Indicated mean effective pressure

**MDDI**: Methanol diesel dual direct injection

**MeOH**: Methanol

**MSOI**: Methanol start of injection timing

**NO:** Nitric oxide

**$NO_x$**: Nitrogen oxides

**PFI**: Port fuel injection

**rpm**: Revolutions pre minute

**SI**: Spark ignitionx

**$SO_x$**: Sulphur oxides

**TDC**: Top dead centre

**uHC**: Unburnt hydrocarbon

## ACKNOWLEDGMENTS

The experiments were performed at the UNSW Engine Research Laboratory, Sydney, Australia. The authors thank Dr Mark Zhai for his significant technical support.

## REFERENCES

[1] Shadidi B, Najafi G, Yusaf T. A Review of Hydrogen as a Fuel in Internal Combustion Engines. Energies 2021;14:6209. https://doi.org/10.3390/en14196209.

[2] Svanberg M, Ellis J, Lundgren J, Landälv I. Renewable methanol as a fuel for the shipping industry. Renewable and Sustainable Energy Reviews 2018;94:1217–28. https://doi.org/10.1016/j.rser.2018.06.058.

[3] White C, Steeper R, Lutz A. The hydrogen-fueled internal combustion engine: a technical review. International Journal of Hydrogen Energy 2006;31:1292–305. https://doi.org/10.1016/j.ijhydene.2005.12.001.

[4] Ayodele TR, Munda JL. Potential and economic viability of green hydrogen production by water electrolysis using wind energy resources in South Africa. International Journal of Hydrogen Energy 2019;44:17669–87. https://doi.org/10.1016/j.ijhydene.2019.05.077.

[5] Lee B, Lee H, Lim D, Brigljević B, Cho W, Cho H-S, et al. Renewable methanol synthesis from renewable H2 and captured CO2: How can power-to-liquid technology be economically feasible? Applied Energy 2020;279:115827. https://doi.org/10.1016/j.apenergy.2020.115827.

[6] Verhelst S, Turner JW, Sileghem L, Vancoillie J. Methanol as a fuel for internal combustion engines. Progress in Energy and Combustion Science 2019;70:43–88. https://doi.org/10.1016/j.pecs.2018.10.001.

[7] Karim G. Hydrogen as a spark ignition engine fuel. International Journal of Hydrogen Energy 2003;28:569–77. https://doi.org/10.1016/S0360-3199(02)00150-7.

[8] Agarwal AK, Valera H, Pexa M, Čedík J, editors. Methanol: A Sustainable Transport Fuel for SI Engines. Singapore: Springer Singapore; 2021. https://doi.org/10.1007/978-981-16-1224-4.

[9] Lee KJ, Kim YR, Byun CH, Lee JT. Feasibility of compression ignition for hydrogen fueled engine with neat hydrogen-air pre-mixture by using high compression. International Journal of Hydrogen Energy 2013;38:255–64. https://doi.org/10.1016/j.ijhydene.2012.10.021.

[10] Shamun S, Haşimoğlu C, Murcak A, Andersson Ö, Tunér M, Tunestål P. Experimental investigation of methanol compression ignition in a high compression ratio HD engine using a Box-Behnken design. Fuel 2017;209:624–33. https://doi.org/10.1016/j.fuel.2017.08.039.

[11] Yao C, Cheung CS, Cheng C, Wang Y, Chan TL, Lee SC. Effect of Diesel/methanol compound combustion on Diesel engine combustion and emissions. Energy Conversion and Management 2008;49:1696–704. https://doi.org/10.1016/j.enconman.2007.11.007.

[12] Sandalcı T, Karagöz Y. Experimental investigation of the combustion characteristics, emissions and performance of hydrogen port fuel injection in a diesel engine. International Journal of Hydrogen Energy 2014;39:18480–9. https://doi.org/10.1016/j.ijhydene.2014.09.044.

[13] Chintala V, Subramanian KA. A comprehensive review on utilization of hydrogen in a compression ignition engine under dual fuel mode. Renewable and Sustainable Energy Reviews 2017;70:472–91. https://doi.org/10.1016/j.rser.2016.11.247.

[14] Dimitriou P, Tsujimura T. A review of hydrogen as a compression ignition engine fuel. International Journal of Hydrogen Energy 2017;42:24470–86. https://doi.org/10.1016/j.ijhydene.2017.07.232.

[15] Wang Q, Wei L, Pan W, Yao C. Investigation of operating range in a methanol fumigated diesel engine. Fuel 2015;140:164–70. https://doi.org/10.1016/j.fuel.2014.09.067.

[16] Park H, Kim J, Bae C. Effects of Hydrogen Ratio and EGR on Combustion and Emissions in a Hydrogen/Diesel Dual-Fuel PCCI Engine, 2015, p. 2015-01–1815. https://doi.org/10.4271/2015-01-1815.

[17] Chintala V, Subramanian KA. Experimental investigations on effect of different compression ratios on enhancement of maximum hydrogen energy share in a compression ignition engine under dual-fuel mode. Energy 2015;87:448–62. https://doi.org/10.1016/j.energy.2015.05.014.

[18] Wang Q, Yao C, Dou Z, Wang B, Wu T. Effect of intake pre-heating and injection timing on combustion and emission characteristics of a methanol fumigated diesel engine at part load. Fuel 2015;159:796–802. https://doi.org/10.1016/j.fuel.2015.07.032.

[19] Song R, Liu J, Wang L, Liu S. Performance and Emissions of a Diesel Engine Fuelled with Methanol. Energy Fuels 2008;22:3883–8. https://doi.org/10.1021/ef800492r.

[20] Boretti A. Advantages of the direct injection of both diesel and hydrogen in dual fuel H2ICE. International Journal of Hydrogen Energy 2011;36:9312–7. https://doi.org/10.1016/j.ijhydene.2011.05.037.

[21] Dong Y, Kaario O, Hassan G, Ranta O, Larmi M, Johansson B. High-pressure direct injection of methanol and pilot diesel: A non-premixed dual-fuel engine concept. Fuel 2020;277:117932. https://doi.org/10.1016/j.fuel.2020.117932.

[22] Liu X, Seberry G, Kook S, Chan QN, Hawkes ER. Direct injection of hydrogen main fuel and diesel pilot fuel in a retrofitted single-cylinder compression ignition engine. International Journal of Hydrogen Energy 2022;47:35864–76. https://doi.org/10.1016/j.ijhydene.2022.08.149.

[23] Saccullo M, Benham T, Denbratt I. Dual Fuel Methanol and Diesel Direct Injection HD Single Cylinder Engine Tests, 2018, p. 2018-01–0259. https://doi.org/10.4271/2018-01-0259.

[24] Zhao Y, Liu X, Kook S. Effect of three-hole nozzle orientations on sprays and combustion in methanol-diesel dual direct injection engines. Applied Thermal Engineering 2024;254:123953. https://doi.org/10.1016/j.applthermaleng.2024.123953.

[25] Zhao Y, Liu X, Kook S. Combustion Mode Evaluation of a Methanol–Diesel Dual Direct Injection Engine with a Control of Injection Timing and Energy Substitution Ratio. SAE Int J Engines 2024;18. https://doi.org/10.4271/03-18-01-0002.

[26] Kook S, Liu X, Edmonds B, Hydrogen-diesel direct injection dual-fuel system for internal combustion engines. Australian Patent Provisional Application No. 2022900118, filed 21 Jan 2022, International Application No. PCT/AU2023/050019, International Publication Date 27 Jul 2023.

[27] Liu X, Srna A, Yip HL, Kook S, Chan QN, Hawkes ER. Performance and emissions of hydrogen-diesel dual direct injection (H2DDI) in a single-cylinder compression-ignition engine. International Journal of Hydrogen Energy 2021;46:1302–14. https://doi.org/10.1016/j.ijhydene.2020.10.006.

[28] Padala S, Kook S, Hawkes ER. Effect of Ethanol Port-Fuel-Injector Position on Dual-Fuel Combustion in an Automotive-Size Diesel Engine. Energy Fuels 2014;28:340–8. https://doi.org/10.1021/ef401479s.

[29] Kook S, Bae C, Miles PC, Choi D, Pickett LM. The Influence of Charge Dilution and Injection Timing on Low-Temperature Diesel Combustion and Emissions, 2005, p. 2005-01–3837. https://doi.org/10.4271/2005-01-3837.

## CONTACT

Mr. Yifan Zhao
The University of New South Wales
Sydney, Australia
chris.zhao@student.unsw.edu.au

Dr. Xinyu Liu
The University of New South Wales
Sydney, Australia
xinyu.liu2@unsw.edu.au

A/Prof. Shaun Chan
The University of New South Wales
Sydney, Australia
qing.chan@unsw.edu.au

Prof. Shawn Kook
The University of New South Wales
Sydney, Australia
s.kook@unsw.edu.au